Kinetic modeling of the jet extraction mechanism in spherical IEC devices

IEPC-2013-416

Presented at the 33rd International Electric Propulsion Conference,
The George Washington University • Washington, D.C. • USA
October 6 – 10, 2013

Georg Herdrich[1], Constanze Syring[2], Marcel Pfeiffer[3],
Institute of Space Systems (IRS), Stuttgart, 70569, Germany

Dejan Petkow[4]
ESA-ESTEC Advanced Concepts Team, Keplerlaan 1, Noordwijk, 2201, The Netherlands

Abstract: The ESA ACT Ariadna study 12/3201 is summarized. The study aims at resolving numerically the effects and phenomena leading to and occurring in a jet extraction inside a spherical Inertial Electrostatic Confinement device. The underlying numerical methodology and software is based on a Particle-In-Cell (PIC) code solving the full set of Maxwell equations coupled with a) a Direct simulation Monte Carlo (DSMC) solver which resolves (mainly, but not only) chemical processes like electron induced ionization of atoms, and with b) a Monte Carlo based Fokker Planck solver (embedded in the DSMC solver) which resolves the Coulomb collision induced relaxation of electron and ion velocity distribution functions. Due to the extremely low time step size necessary to guarantee numerical stability of the PIC solver the simulation domain is downsized. This speed-up process demands the definition of proper inflow boundary conditions. These conditions are derived on basis of available literature and scaling laws. Other main speed-up measures are neglecting of Coulomb collisions as well as ionization processes. The eventual outcome is the simulation and visualization of the electron jet and the preemptive development of the ion jet on basis of an assumed ion saturation zone near the centre. Recommendations for further simulations and studies are given and more detailed simulations of the jet are proposed.

Nomenclature

B	=	magnetic flux density
d_a	=	anode diameter
d_c	=	cathode diameter
$d_{a,O}$	=	jet grid opening in anode grid
$d_{c,O}$	=	jet grid opening in cathode grid
Δv	=	velocity increment/change
Δt	=	time increment/change
E	=	electrical field
E_{bg}	=	background electrical field
E_{in}	=	charge induced electrical field
f_a	=	velocity distribution function of species α

[1] Head Plasma wind tunnels and Electric Propulsion, Space Transportation, herdrich@irs.uni-stuttgart.de.
[2] Research Associate, Plasma Wind Tunnel and Electric Propulsion, syring@irs.uni-stuttgart.de.
[3] Research Associate, Plasma Wind Tunnel and Electric Propulsion, pfeiffer@irs.uni-stuttgart.de.
[4] Research Fellow, ESA Advanced Concepts Team, dejan.petkow@googlemail.com.

f_β	=	velocity distribution function of species β
F	=	external force(s)
g	=	relative velocity (between particles of species α and β)
I_{PS}	=	current (power supply related)
j	=	current density
m_α	=	mass of particle α
$n_{e,c}$	=	number density of electrons in core
$n_{i,c}$	=	number density of ions in core
n_n	=	number density of neutrals
P_k	=	location of nodes
ρ	=	density
σ_D	=	collision cross section
t	=	time
T_e	=	electron temperature
T_i	=	ion temperature
τ_{ee}	=	collision time between electron and electron
τ_{ei}	=	collision time between electron and ion
τ_{ii}	=	collision time between ion and ion
τ_{en}	=	collision time between electron and neutral
τ_{in}	=	collision time between ion and neutral
τ_{nn}	=	collision time between neutral and neutral
x	=	coordinate
	=	position vector
v	=	velocity species α
V_a	=	anode voltage
V_c	=	cathode voltage
V_{ch}	=	chamber volume
W	=	velocity species β
Φ	=	electrical potential
Ω	=	solid angle
TL	=	time passed for top left image
TR	=	time passed for top right image
BL	=	time passed for bottom left image
BR	=	time passed for bottom right image

I. Introduction

The inertial electrostatic confinement (IEC) of ions for the purpose of creating a high density (fusion) plasma was first studied experimentally by Hirsch [1] in 1967 and originally proposed by Farnsworth [2]. However little was done to study this concept until R.W. Bussard [3] and G.H. Miley [4] renewed studies in the early 1990s. There are several design types of IECs, e.g. single-grid devices [5], multiple-grid designs [6] or a hybrid magnetic-electrostatic version [3]. All these experiments are fusion power concepts, yet no break-even for the energy production is expected from the concepts introduced here. But due to the design simplicity and scalability, development was still pursued and research done over decades aimed to increase the fusion rates as much as possible, so that they can be used e.g. as commercial neutron sources [7] as it was planned by Daimler-Chrysler Aerospace (IEC star-mode fusion neutron source, R&D). Today, Gradel sarl (Project "NSD Gradel Fusion", formerly the NSD Fusion GmbH) pushes in Europe the enhancement of commercial IEC devices amongst other things for luggage inspections or neutron radiography.

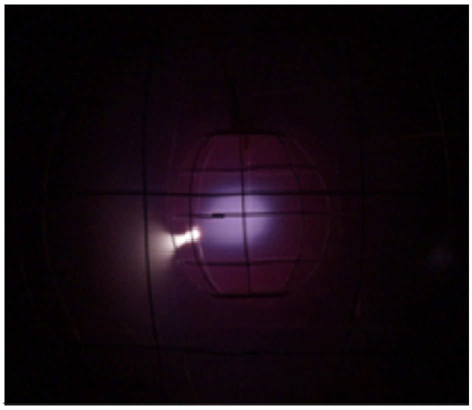

Figure 1. IRS IEC in jet mode.

With begin of 2010, a project was set up to build up an IEC test stand in the IRS Laboratory which shall help to broaden the understanding and knowledge about inertial electrostatic plasma confinement and related plasma beam extraction [8]. Figure 1 shows the IRS IEC in operation (jet mode). This development activity is embedded in the IRS electric and advanced space propulsion developments [9]. A strong motivation for this consists in the fact that IEC seems to be promising in terms of high specific impulses. In addition, systems run in fusion mode may be promising alternatives for energy supply systems with the particular advantage that the confinement technology has a positive mass trade-off compared with classical magnetic field based confinement systems.
Moreover, a plasma simulation tool for investigating highly rarefied gas and plasma flows is permanently under development since 2004/05 and applied to study phenomena leading to the plasma jet extraction. Available scientific literature on IEC with and without jet extraction states that grid transparency is increased with respect to what is state of the art in gridded ion thrusters, thus promising lower grid erosion and, hence, increased life times. However, literature on IEC in jet mode contains very little details regarding the underlying physics which lead to the jet extraction. Even worse, a comprehensive experimental jet characterization allowing deriving reliable comparative conclusions (with respect to state of the art electric propulsion devices) is currently not available. Correspondingly, not only jet extraction is not really understood, but also stated thruster properties contain a significant portion of speculation and anticipation. It is the intention of this study to improve our understanding of the IEC technology and certainly of the jet extraction mechanism as key to the IEC's usability as a space propulsion device. The method of choice is to apply a numerical code which is able to resolve the relevant physics with adequate accuracy.

II. IEC set-up and function

Both set-up and function of the IEC system investigated are introduced here. This may be a help to improve the understanding of the approach that was chosen in this study.

A. IRS IEC set-up

The IEC in its simplest form is a one grid system that makes use of the chamber wall as outer electrode. However, a two-grid system as investigated at IRS stems two significant and important aspects:

- With a two-grid system the IEC system can be considered as an independent set-up representing the point of departure for the consideration of the IEC as a separate potential advanced energy supply and/or propulsion system.
- The easy to manipulate two-grid electrode system enables both numerical and experimental parameter studies e.g. on basis of geometry variations of the electrodes.

For the phase 1 investigations, see Fig. 2, the IRS experimental IEC test stand is dedicated to assess an understanding of the basic discharge behavior and confinement modes. The anode grid has a diameter of 30 cm, the cathode grid of 10 cm. A maximum voltage of 4 kV can be applied to the cathode with the current 500 W power supply. It is planned to go up to 7 kV which is the maximum allowed voltage for the electrical feed through system of the vacuum chamber. The vacuum facility with the dimensions of 1 m diameter and a length of 2,75 m has the capability of a base background pressure of 10^{-5} hPa using the 3-stage pumping system of the facility. The flow of neutral gas through the chamber is controlled by a 1 slm gas flow controller. Correspondingly, and the chamber pressure is set by the flow and pumping speed.

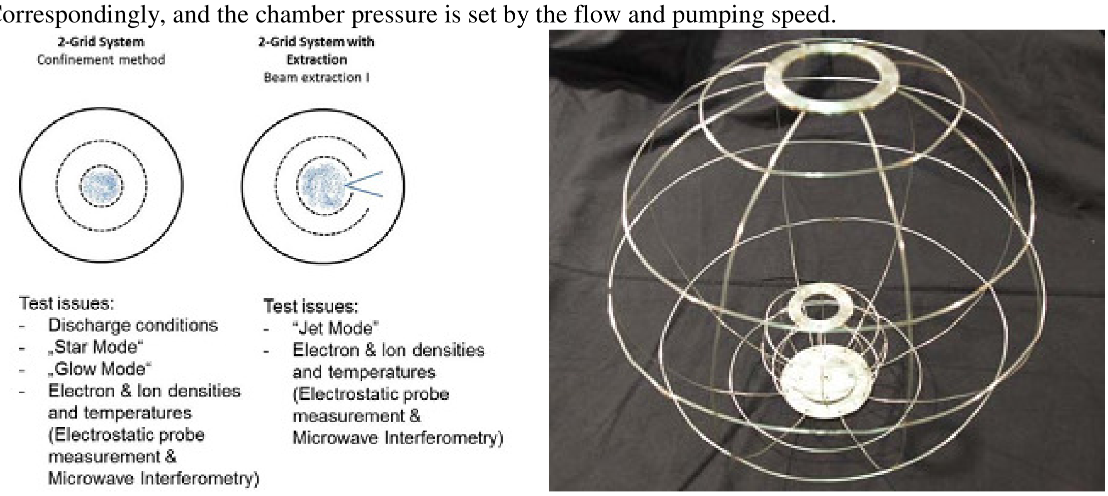

Figure 2 Left: Schematic for phases 1 and 2; right: a two-grid IRS IEC set-up (so-called C1-grid, see [10]).

The anode grid consists of 4 ring shaped wires in latitude direction and 5 in longitude. For the cathode 4 longitude rings and 3 latitude rings are used. The 1 mm wires are spot-welded forming the longitude-latitude system (see Figure 2, right side) with a geometric transparency of ~ 95 %. Meanwhile smaller grid systems are under investigation at IRS as well. The interested reader may refer to reference [10].

B. IEC working principle

In the case of the IRS set-up basically a glow discharge is produced by the time the electrodes are set to a significantly leveled voltage / potential. In the reference condition that has a voltage of the order of 1 kV and typical pressures roughly below 1 Pa this leads to an E/p value of about 50 kV/(m·Pa). This clearly indicates that T_e is significantly larger than the heavy particle temperatures [11].

The negative voltage allows for an acceleration of the positively charged Argon ions in the direction of the cathode. This circumvent in combination with the significant transparency of the cathode enables that ions with respective kinetic energy may pass the cathode and enter the core of the IEC. In fact, the process at the whole may be dynamic depending on the kinetic energy of these ions. Ions that do not have enough energy are trapped in the core, while others with high kinetic energies may pass the core and leave it "on the other side" of the cathode grid. If this happened they would be attracted again by the cathode which may lead to a repetition of the aforementioned ion movement provided that the ion is not kept at the surface of the cathode where it would be neutralized. Eventually a significant amount of ions is then trapped in the core and the process lasts until an equivalence between the external Coulomb forces (due to the cathode's potential) and the internal Coulomb forces (space charge limitation of the ions in the core) is produced.

Consequently, the internal energy of the ions that are trapped in the core is significantly high (in our reference case in the order of 600 MJ/kg). A local asymmetric configuration of the electrodes may produce gradients in the electrical potential that at least trigger the electrons to form a jet. In diverse literatures well educated guesses express that the ions then follow the electrons. From the results of this study it is rather believed that the high energy densities in the core somehow expand thermally and, moreover, the micro fields that accompany the quasi neutrality violation let the ions follow the path of the electrons. The Debye lengths in combination with the results of this study, however, imply that the electrons do not sufficiently attract the ions meaning that a jet extraction effect as such can be excluded.

III. Introduction to simulation software

In 2005, an academic cooperation was founded between the Institute of Aerodynamics and Gas Dynamics (IAG) of the Universität Stuttgart, the High Performance Computing Center Stuttgart (HLRS), the Institute of Space Systems (IRS) of the Universität Stuttgart, and the Karlsruhe Institute of Technology (KIT). The goal was to numerically study the acceleration phenomena inside a non-stationary magnetoplasma-dynamic thruster [12]. Due to certain thruster properties the main software requirements were identified as follows:

- 3D capability,
- fully kinetic solution approach,
- particles are (also) treated relativistically,
- all Maxwell equations are solved (this also includes the divergence conditions for E and H),
- chemistry is included and
- collisional relaxation of electrons and ions is modeled.

The term fully kinetic implies that, as in most kinetic approaches, the plasma is represented by a sample of different species of charged particles. In each time step the electromagnetic fields obtained by the numerical solution of the Maxwell equations at the grid are interpolated to the actual locations of these particles. According to the Lorentz force the charges are redistributed and the new phase-space coordinates are determined by solving the usual laws of dynamics. To close the chain of self-consistent interplay, the particles have to be located with respect to the computational grid in order to assign the contribution of each charged particle to the charge and current density at the nodes which are the sources for the Maxwell equations in the subsequent time step. Given that, the presented approach is a combination of two different frameworks:

- Eulerian framework: discretisation of Maxwell's equations on fixed interpolation points,
- Lagrangian framework: discretisation of the species' distribution functions (in principal the trajectories of the system of particles are derived).

These frameworks are coupled and interact with each other via the charge-to-grid and force-to-charge assignment steps. Such a basic scheme is the starting point to build up the necessary program structure of the coupled code which allows for flexible combination of different modules and extensions. In fact, the code is able to solve kinetically the complete and fundamental gas kinetic.

A. Governing equations and domain codes

The governing equation for rarefied gases is the Boltzmann equation:

$$\frac{\partial f_\alpha}{\partial t} + v\frac{\partial f_\alpha}{\partial x} + \frac{F}{m_\alpha}\frac{\partial f_\alpha}{\partial v} = \int_{-\infty}^{\infty}\int_0^{4\pi}\left[f_\alpha(v')f_\beta(w') - f_\alpha(v)f_\beta(w)\right] g\sigma_D d\Omega dv \qquad (1)$$

Equ. (1) describes the evolution of the velocity distribution function f_α of species α scattered by a background species β with the velocity distribution function f_β. The left side describes the change of f_α over time t, the dependence of f_α on spatial inhomogenities, and the change of f_α as a consequence of external (i.e. non-collisional) forces F accelerating the particles of the species α with the mass m_α. The right side depicts the change of f_α due to inter-particle collisions. Collisions are described by the collision cross section σ_D which depends on the relative velocity g between both particles. Post-collisional quantities are primed. The mathematical solution of equ. (1) is difficult and a typical approach is to split the equation in domains e.g. when collisional processes can be neglected the so-called Vlasov-equation results. Together with the force terms this equation describes the collective plasma phenomena. The most established kinetic solver in this domain is the particle-in-cell solver (PIC) which is also used in the investigations presented here.

Collisional processes can be characterised by the mean collision time τ which typically follows this order:

$$\overbrace{\tau_{ee} < \tau_{ei} < \tau_{ii}}^{small\ angle\ scattering} \quad < \quad \underbrace{\tau_{en} < \tau_{in} < \tau_{nn}}_{large\ angle\ scattering} \qquad (2)$$

The indices describe the charge related nature of the particles (i.e. electron, ion, neutral). As can be seen in equ. (2) the order of the collision frequency is related to the scattering angle of a single collision process. Therefore, two different solver types have been established by the corresponding communities: Fokker Planck (FP) solvers solve the Fokker Planck equation which can be derived from the RHS of equ. (1) assuming small scattering angles. All other scattering processes can be covered kinetically by e.g. the Direct Simulation Monte Carlo (DSMC) approach. Both a Monte Carlo based FP solver and a DSMC solver have been developed in order to resolve all plasma phenomena on all scales by coupling to a PIC solver.

B. Code coupling

Depending on the level of fidelity and / or assumptions possible the simultaneous application of the domain codes is justifiable also from the point of view of computer resources to be allocated. Correspondingly, often certain aspects of the problem are already described adequately if the solver system is reduced. Often, however, the user is forced to artificially reduce the problem either due to limited computer resources and/or due to a lack of data e.g. in the field of boundary conditions.

The coupling scheme for all the three domain codes is depicted in Fig. 3. The three different solvers (PIC, DSMC, and FP) are aligned in a parallel fashion describing the mutual independency during the computation. However, each solver produces information on the change of the particle velocities treated in the respective solver such that, all velocity change contributions are considered.

A detailed description of the solvers can be found in reference 11.

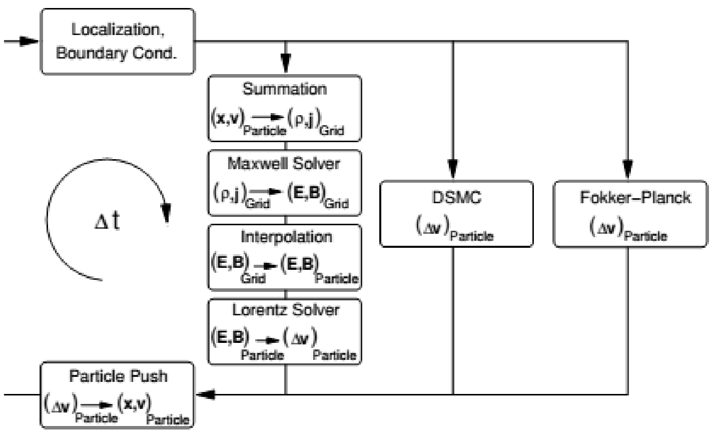

Figure 3. Cycle of PICLas time step.

IV. Assessment of initial particle data: Literature review and respective analysis

For an adequate simulation, realistic input parameters are needed to initiate the particle interactions and motions. The originally stated problem cannot be treated with the applied kinetic code due to a severe mismatch between the corresponding computational needs and the available resources in the frame of the ESA Ariadna study. Hence, a two staged downsizing of the simulation domain was introduced: Firstly, the overall IEC device was shrinked by a factor of six with respect to the anode diameter. Secondly, only a box covering the inter-electrode jet stream and parts of the plasma core including the cathode's grid opening is simulated, see below. This simplification procedure imposes the identification of matching inflow particle properties which cannot be derived from literature without further assumptions and scaling laws.

A. Reviewed IEC configurations

The publications depicted in table 3.1 for ion and electron density measurements have been reviewed using spherical inertial electrostatic confinement devices and cylindrical electrostatic confinement devices in pulsed and steady-state operation. These references include measurements of averaged electron density or electron density profiles with microwave Fabry-Perot [14, 15] or Laser heterodyne interferometry [15, 16] and also electrostatic probe measurements [17] within the cathode grid.

A database has been established from all this data. Given that the IEC setup at IRS is based on two spherical electrodes with a steady-state Argon based glow discharge, the data published by Dobson and Hrbud [14] was selected as reference configuration although the data base in [14] is still incomplete. This decision was additionally motivated by the fact that the data set, incomplete though, is the largest compared with the other data sets and, moreover, personal contacts to the authors (for communication and clarification purposes) exist. Table 1 exemplarily shows 4 set-ups investigated within this review. The synthesis of respective data such as number densities increased the confidence level on the expected order of magnitudes of these densities.

Table 1: IEC set-ups reported in literature; reference 12 is reference for the investigations in this work

	Meeker et al. [15]	**Dolan [16]**	**Dobson, Hrbud [14]**	**Thorson [17]**
Shape	cylindrical	cylindrical	spherical	Cylindrical
Plasma generation	Electron impact (oxide cathodes)	Electron impact (oxide cathodes)	Glow discharge	Electron impact (tungsten filaments)
Propellant	Deuterium	Neon	Argon / Deuterium	Hydrogen
Grids	2	2	2	3

B. Reference Conditions used for simulations

The four different conditions investigated in [14] are separated in 2 conditions for Argon and 2 conditions for Deuterium. For simplicity reasons and due to the fact that the IRS facility has been operated with Argon as well it was decided to take Argon as a reference. Moreover, the applied voltages for the IRS facility are almost the same (-1 kV). Geometries and further parameters are depicted in table 2. The electron number densities with the bracket (exp.) in table 2 are derived from microwave interferometry taken in the IEC core, see [14]. The derived electron number densities were between 0.4 and $7 \cdot 10^{16}$ m^{-3}. The numerical simulation of the one-dimensional Poisson equation and energy distribution functions yielded rather flat profiles.

Table 2: Reference conditions for the simulations performed

	Working gas	**V_c [kV]**	**V_a [kV]**	**I_{PS} [mA]**	**d_a [m]**	**d_c [m]**	**V_{ch} [m^3]**	**$n_{e,c}$ 10^{16} [m^{-3}]**
	Argon	-1.01	0	50	0,6	0.23	0.905	2.6 (exp.)
								4.031 (num.)
Ref.	[14]							
	$n_{i,c}$ 10^{16} [m^{-3}]	**n_n 10^{16} [m^{-3}]**	**T_i / K**	**T_e / K**				
	- (exp.)	$1.93 \cdot 10^4$	300	10000				
	4.04 (num.)							
Ref.	[14]							

For the sake of consistency the numerically derived values for the core electron and ion density were taken. The neutral particle density n_n is derived from the chamber background pressure and an assumed neutral particle temperature of 1000 K. For a typical glow discharge the neutral particles can be assumed to have almost room temperature. The 1000 K in turn account for the microwave heating effects. Moreover, the sensitivity of n_n is rather small with respect to temperature changes in a range between 300 K and 1000 K. The significance of secondary electrons was investigated in [13]. This led to the overall neglecting of electrons as such for the majority of relevant processes. An exception may be neutral-ion collisions where the outcome was that this may be a source of electrons in the core of the IEC. However, this is subject of future investigation as the current data base does not provide enough information to derive an adequate assumption.

All assumptions assessed for the secondary electrons but also at the whole should be verified in further studies as this is outside the scope of this project. In all simulations, electrons have been initialized with T_e = 1300 K. Despite the fact that this number is not justified by reference or own concrete estimations, a sensitivity analysis has shown negligible difference in the results compared to T_e = 10000 K. The latter is an upper limit estimation keeping in mind the different sources (primary vs. secondary electrons). The low impact of the choice of initial electron temperature is due to the impact of the electric field on electron energy with respect to thermal movement. Hence, assuming T_e = 1300 K is considered an acceptable estimation.

The acceleration of ions from anode to the cathode can be estimated assuming a planar electrode configuration. The initial radial ion velocity component equals then $v_i = (2q_iV_c/m_i)^{0,5}$ with the particle charge q_i, cathode voltage V_c (assuming the anode is grounded) and ion mass m_i. After a couple of passes through the plasma core including elastic scattering with other particles, the accelerated ions are lost to either the grid or to so-called charge exchange reactions with their neutral counterparts. A quantification of this highly dynamic process is currently impossible such that the average macroscopic velocity (v_i = 0 m/s) of these ion oscillations are applied during initialisation. Acceleration processes depend solely on external electric fields as well as on inter-particle interactions provided by the PIC solver.

Electrons drifting outside the cathode are neglected. Neutrals are assumed to remain basically static between the electrodes so their velocities are neglected as well.

V. Assessment of initial geometry data

This chapter summarises the activities and decisions made leading to the final simulation domain. Due to the high accuracy of the Maxwell solver the initially identified reference geometry was down scaled twice. First, the grid dimensions were reduced by a factor of six according to the anode's diameter, see below. The Maxwell solver's output is reduced to the electric and magnetic fields generated by the charges in the plasma while the external electric field is provided by a proper tool.

A. Reference simulation regime set-up

Current literature does not provide a proper reference by means of a sufficiently studied IEC plasma configuration including both grid openings leading to a jet extraction and respectively determined plasma parameters.

Table 3: Reference grids and simulation set-up

	Meyer [18]	Dobson, Hrbud [14]	Simulation set-up
d_a	0.457 m	0.6 m	0.1 m
d_c	0.095 m	0.23 m	0.034 m
$d_{a,0}$	0.142 m		0.024 m
$d_{c,o}$	0.04 m		0.0066 m

Therefore, the following procedure was developed: Meyer [18] provides geometric grid information for jet extraction but no reliable plasma properties unlike Dobson and Hrbud [14] which provide useful plasma data but measured in a standard IEC configuration.

Since the detailed grid with its wires and spacings is not included in the simulation grid the ratio of grid spacing to grid opening for the jet will not have an impact, but the ratio of the jet grid opening in cathode grid $d_{c;O}$ to jet grid opening in anode grid $d_{a;O}$ will, see Fig. 4. Assuming that the grid openings scale according to Meyer [18], hypothetical grid openings can be devised for the IEC configuration of Dobson and Hrbud [14] which is then scaled down by a factor of six with respect to the anode's diameter da in order to reduce computational load, see Tab. 3. Of course, this method implies the assumption that neither the scaling of the grid openings nor the down scaling of the whole IEC setup affects the measured plasma properties identified in Dobson and Hrbud [14].

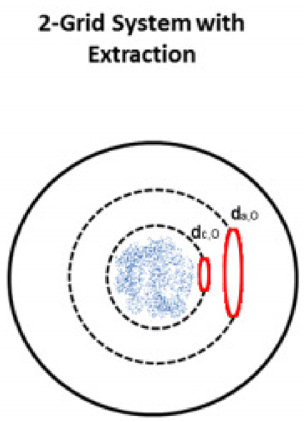

Figure 4. IEC set-up with grid openings.

B. Electrostatic background field calculation

In general, the total electric field E which is seen by a charge is a superposition of the local electric background field and the field caused by all other charges in the computational domain. In case of the IEC, potential boundary conditions are required, i.e. it is necessary to define a voltage on the acceleration grids to obtain the electric background field according to.

$$\vec{E} = -\nabla\Phi. \qquad (3)$$

However, the transient Maxwell solver algorithmically does not allow to incorporate a potential boundary condition, only E_i or $\partial_{xi}E_i$ for i = 1; 2; 3 is possible. To circumvent this problem the electric field calculation is separated into the calculation of the background field E_{bg} and the electric field E_{in} induced by the charges in the plasma. Once both values are known throughout the domain (i.e. on all grid points), they are superimposed. This procedure implies that the plasma does not affect the boundary conditions due to the constantly applied grid voltage. Hence, E_{bg} is calculated once in the beginning of the simulation and remains constant. The electrostatic background field is generally obtained by solving the Laplace equation

$$\Delta\Phi = 0 \qquad (4)$$

for given boundary conditions (applied voltage, e.g. 1 kV) while no charged particles are inside the simulation domain. Technically, an external open source based solver (OpenFOAM - electrostaticfoam) is used. The work flow for the calculation of equ. 4 can be described as follows:

- Use OpenFOAM to solve equ. 4 with potential boundary conditions, and
- transfer of the background field to the particles via interpolation.

The interpolation of the field data from the mesh to the particles is performed in the following way: For every node of a hexahedral element a value for $\overrightarrow{E_k}$ = [E_x; E_y ; E_z], for k = 1…8 is stored. A particle located at $\overrightarrow{x_i}$ = [x_i; y_i; z_i] in the element is affected by the background field $\overrightarrow{E_i}$ according to

$$\vec{E}_i = \frac{\sum_{k=1}^{8}\sqrt{|\overrightarrow{x_i}-\overrightarrow{P_k}|}\vec{E}_k}{\sum_{k=1}^{8}\sqrt{|\overrightarrow{x_i}-\overrightarrow{P_k}|}}. \qquad (5)$$

This procedure is comparable to a volume-weighting in case of a Cartesian grid.

The original IEC grid geometry is a huge challenge for mesh generators. The spherically arranged small wires lead to a huge number of small mesh cells close to the wires' surface. This is impracticable for most mesh generators and only processable in a huge amount of time. Therefore, we use two spherical shells with respectively one hole for the jet extraction as geometry, see Fig. 5. The complete OpenFOAM mesh has 65600 hexahedral cells.

The only significant difference of the electric field between this geometry and the original IEC geometry will be close to the sphere shells. But the non-symmetric E field which affects the particle motion should be comparable since the focus is on the jet extraction. The boundary conditions for the OpenFOAM simulation are:

- Outer sphere with geometry data listed in Tab. 3 and the potential V_a = 0 V ,
- Inner sphere with geometry data listed in Tab. 3 and the potential V_c = 1 kV,
- Volume is defined as vacuum in a box with the edges 0.12 · 0.12 · 0.12 m^3.

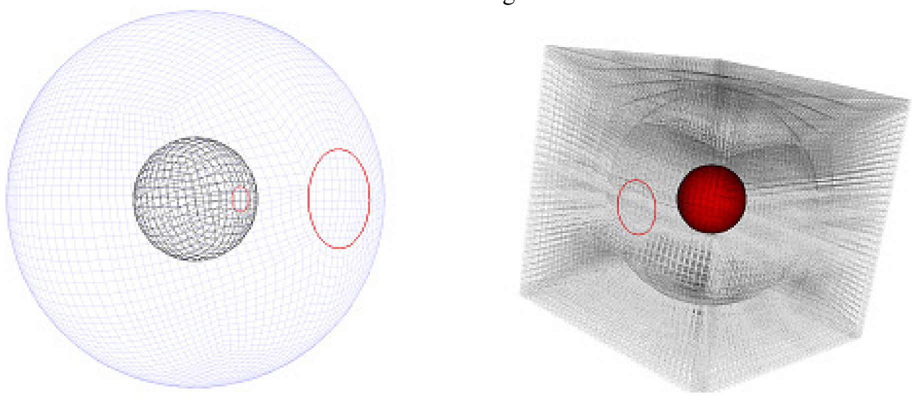

Figure 5. Left: Surface mesh of the two spherical shells with the holes (red).Right: The whole simulation mesh with depicted cell structures, the inner sphere, and the hole of the outer sphere (red).

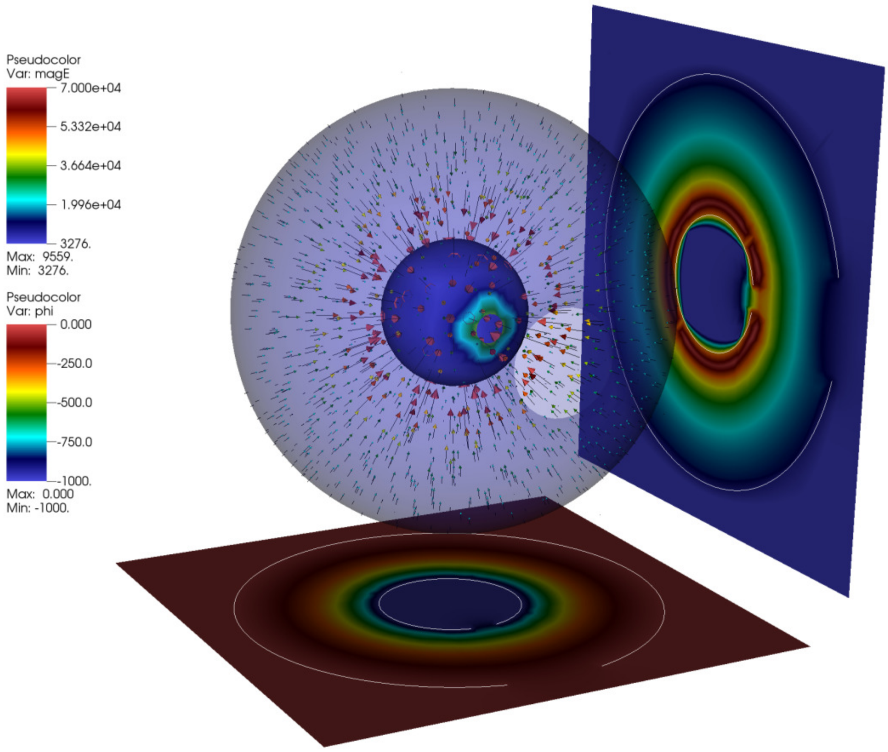

Figure 6. The arrows show the electric field vectors, their colors and lengths are scaled by the electric field's magnitude. Slices through the center showing the magnitudes of the electric field (right) and of the electric potential (bottom).

The results of the OpenFOAM simulation are shown in Fig. 6. The results are as expected. The electric potential is approximately constant inside the inner sphere and outside the outer sphere. Accordingly. the electric fields are very small there. Figure 6 shows that the electric field in the inner sphere does not vanish completely. This is important for the jet extraction of the particles. Especially the streamline plot of the electric field vectors, starting in the inner sphere, is interesting. The plot provides information about the hypothetical (i.e. non-disturbed by other phenomena) stream path of particles accelerated in the inner sphere by the external electric fields.

C. Final simulation domain

The whole two grid system will not be simulated due to the respective computational needs. Therefore, a smaller simulation domain covering the jet extraction volume is considered, see Fig. 8. A new hexahedral grid was defined for this region. The solution of the OpenFOAM solver was then transferred from the original mesh to the new but smaller mesh. For this purpose, a tool was developed that cuts out a subregion of the OpenFOAM solution and interpolates the electric field values from the nodes of the old mesh to the nodes of the new mesh. The interpolation is realized similarly to equ. 5 where the particle positions correspond now to the new mesh's nodes. The work flow is shown in Fig 8. The new hexahedral mesh with the symmetrically structured cells reduces the computational demand further. The smaller and the more warped the cells are (as in the original OpenFOAM mesh close to the sphere shells and the holes), the smaller is the global time step for a stable Maxwell solution. With the original mesh, a maximum time step of about 10^{-16} s is necessary for a stable Maxwell solution. The new mesh allows a time step of about 10^{-12} s.

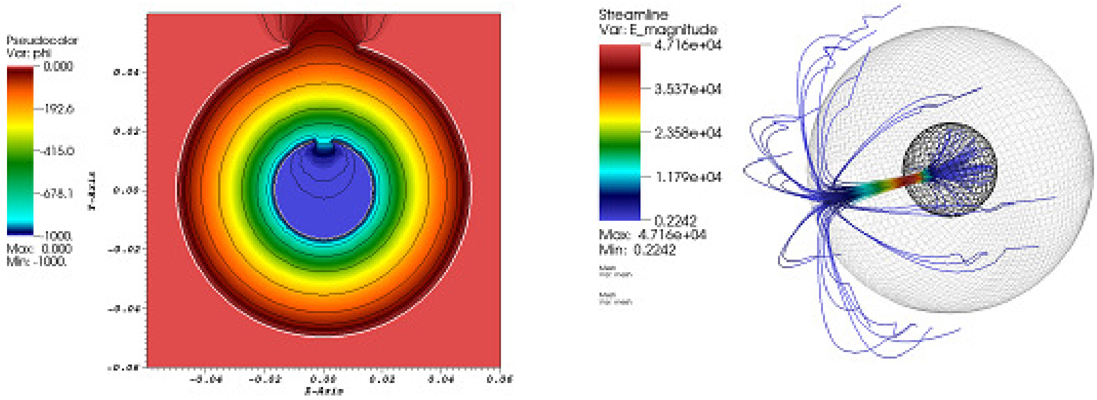

Figure 7. Left: A slice through the center of the magnitude of the electric potential with equipotential lines and a skewed data scale (color table) to show the small variations of the electric potential in the inner sphere and outside the outer sphere. Right: A stream line plot of the electric field vectors that starts in the inner sphere.

For the upcoming simulations an extensive preparatory simulation package had to be performed in order to assess the required

- Spatial descritisation.
- Particle discretisation,
- Shape functions,
- Assessment of a CMC method to reduce computational efforts.

These activities and their respective outcome could fill an own paper and are omitted at this point for the sake of briefness. The careful reader may refer to reference [13] where the preparation activities are explained in detail.

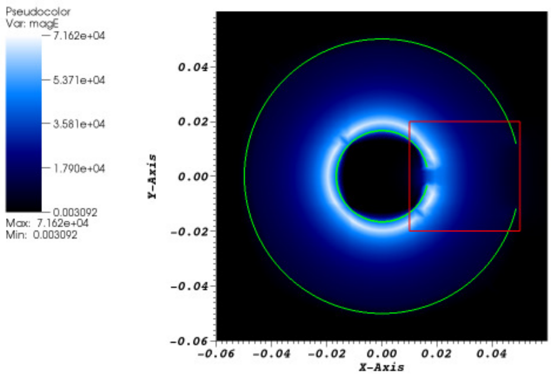

Figure 8. Magnitude of the electric field with the original spherical geometry (green) and the final simulation domain (red).

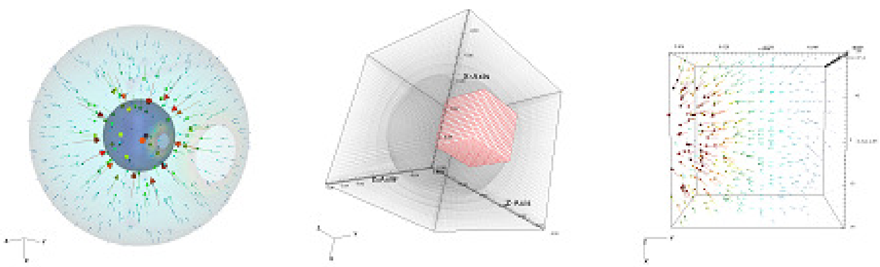

Figure 9. Left: Original electric field vectors with the two IEC spheres. Middle: New simulation mesh (red) on the corresponding position in the old original mesh (black with opacity). Right: New electric field vectors cutted from the original mesh.

VI. Main simulation results

This chapter condensates the most important results as described in detail in reference [13]. Results shown here are performed using the PIC solver only. The reasons for this are manifold e.g. the hybridized simulations with a CMC code (Continuum Monte Carlo) led to results that were physically not reasonable. This is most likely due to the fact, that the boundary conditions as derived from the rare literature and respective processes e.g. in terms of ionization are too unknown. The interested reader is asked to refer to reference [13].

A. Movement of charged particles

The temporal evolution of the electron density is exemplarily shown for ne = $4\cdot10^{16}$ m^3 in Fig. 10. An electron jet is clearly visible. This jet is dominantly created by the electric field which is more or less followed by the electrons.

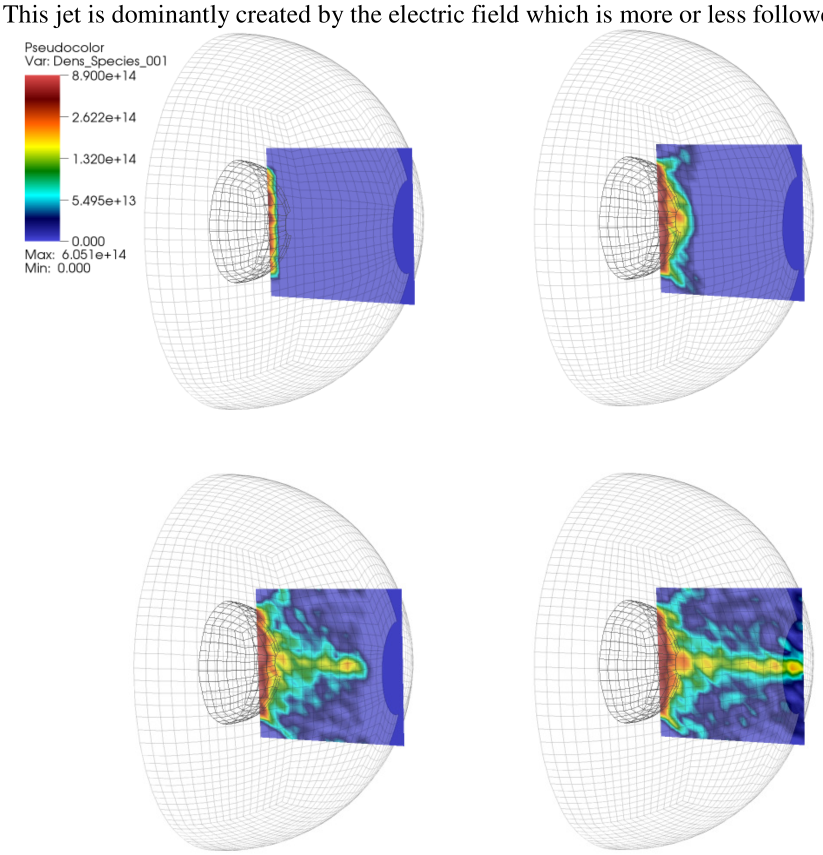

Figure 10. Temporal evolution of the electron density in the simulation region for $n_e = 4\cdot10^{16}$ m^3. TL: $4.3\cdot10^{10}$ s, TR: $1.5\cdot10^{9}$ s, BL: $2.6\cdot10^{9}$ s, BR:$5.2\cdot10^{9}$ s.

Corresponding to the experimental results also an ion jet extraction is expected. To study the ion movement, it is necessary to increase the simulation time because of the greater mass and inertia of the ions. The results of the longer simulation time (24h with 32 processes) are shown in Fig. 11. A region is visible (next to the outer sphere) in which the external electric field and the space charge of the ions cancel each other out. Uniformly distributed ions on the left hand side of this region are all accelerated toward the IEC center and an ion jet is not (yet) formed. More interesting are the electrons on the right hand side of this region. They do not form a jet but they are moving against the external electric field. So, it is probable that the missing Lorentz forces (because of the charges in the regions of the IEC that are not simulated) are obviously necessary for a physical correct simulation and a movement of all the ions against the external electric field. Moreover, the respective sources of ionization are not fully understood. A respective production rate of ions e.g. in the core could lead to significantly high micro fields that may enable that the process shown in Fig. 11 could continue.

However and unfortunately, the simulation of the whole IEC is not feasible during the project time.

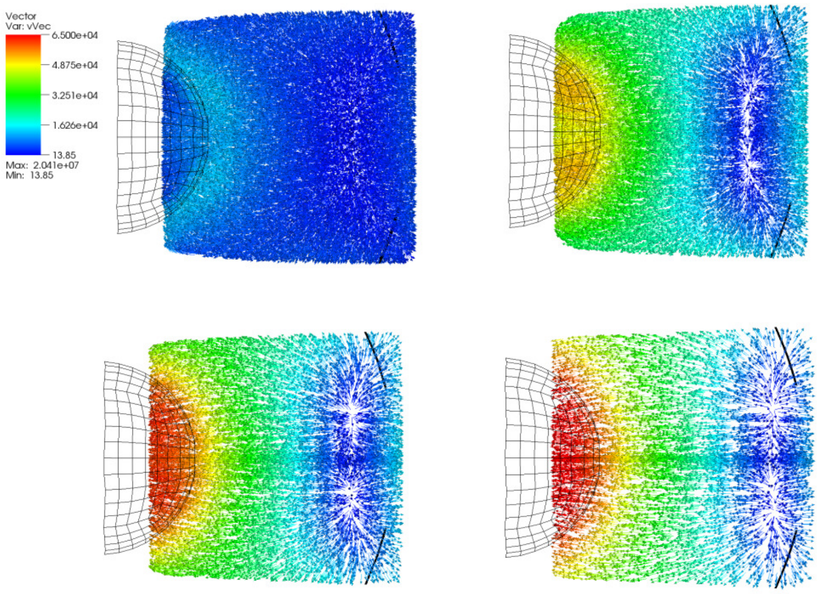

Figure 11. Temporal evolution of the ion velocity vectors for uniformly distributed ions $n_i = 8{\cdot}10^{16}$ m^3. TL: 70 ns, TR: 400 ns, BL: 600 ns, TR: 850 ns.

VII. Conclusion

A sub-domain of a spherical Inertial Electrostatic Confinement thruster was modeled and simulated with a fully kinetic particle based software framework. Externally applied electric fields resulting from electrode geometries and voltages were modeled via OpenFoam, imported into the kinetic code, and treated as local background fields.

Additional electric field information is provided due to the non-collisional interaction between charged plasma particles. The full set of Maxwell's equations was solved to derive resulting forces acting on the particles, thereby enabling a self-consistent treatment.

The electron acceleration as the presumably initialising element of the overall jet extraction was recovered by the kinetic simulations. However, due to issues related to some code modeling elements, the complete jet extraction including ions (which provide the main thrust) was not observed. Hence, we conclude that our simulations provide additional evidence which supports the common theory - that electrons are overcoming the potential barrier. Further elements of the beam extraction hypothesis cannot be confirmed, but also not refuted. Consequently, the main objective of this study - the kinetic simulation of an IEC jet extraction, was achieved only partially. Limiting factors in the modeling are mainly related to the accuracy of the PIC solver which, in its current state, solves the full set of Maxwell equations and, therefore, demands temporal resolution of the vacuum speed of light in the smallest cell in the whole simulation domain. This leads to extremely small time step sizes and, correspondingly, to high computational needs. Although it was possible to further reduce those during the Ariadna project (e.g. no Coulomb collisions, reduction of computational domain) only a limited amount of physical time could be reproduced despite the use of a multi-processor computer architecture.

The reduction of the computational domain reduced the computational needs significantly but this approach imposed the definition of an inflow boundary condition which has a severe impact on the simulation result. As suggested by literature, the behavior of the electrons close to the inner grid opening is driven by the local electrostatic potential which is generally unknown and key outcome of a full domain simulation.

By defining two inflow boundary conditions (representing limiting cases), the potential field's shape and its impact on the electrons was defined artificially. Although the choice of the non-neutral inflow boundary condition over the neutral one based on physical considerations, this limiting case does not reproduce the jet extraction in the applied number of iterations. Note, however, this does not automatically imply that this boundary condition fails in general. A significantly longer simulation time might have led to the desired observations. However, a simulation of a larger (or even the full) physical domain with even less time steps might have lead to the desired observation as well. Both scenarios were in conflict with the available simulation budget which had to be spent mainly for the preparatory simulations for adjusting numerical parameters according to the stated problem. The following table provides an overview of the goals of this study.

VIII. Outlook

Future research activities should focus on improving computational efficiency of the PIC solver. To be precise, a pure PIC solver solving the electrostatic Poisson equation would allow to increase the global time step size by probably 2-3 orders of magnitude with respect to the herein applied PIC solver which resolves the electromagnetic wave propagation. An electrostatic PIC solver would resolve enough physical phenomena relevant to the beam extraction. In fact, this would not only allow to obtain simulation results based on significantly longer physical times but to simulate the whole domain (maybe even non-downsized) in order to provide the natural electrostatic potential distribution close to the inner grid opening. This would also relax the need for significantly more accurate particle data which needs to be provided as initial and boundary condition in the current numerical setup. However, smaller speed-up values are expected making use of the newly developed and implemented but not yet verified pseudo-electrostatic Poisson solver.

The plane which represents the exit face of the jet particles should contain some clever algorithm which is able to cope with the charges already left the domain (at least to some degree of accuracy) but still having electrostatic impact on the charges inside the domain. Currently, a charge leaving the system does not have an impact on any charge inside the domain despite the long range Coulomb potential. Also, the role of Coulomb collisions near the inner grid opening should be studied more in detail as well as chemical reactions which affect the composition of the jet. In fact, the electron distribution function' relaxation is coupled to the chemistry due to the fact that electron induced processes are much more efficient than ion induced reactions. The inclusion of nuclear fusion reactions would allow to answer whether a mode of operation exists which justifies to operate an IEC thruster in a hybrid jet and fusion mode. Given that, a Fokker Planck solver would presumably impact on the resolution of space charge induced jet extraction processes (to get a full picture of the acceleration process), on the chemical processes along the jet stream (to assess beam properties and thrust characteristics), and on the thermalisation of highly energetic charged nuclear fusion products (to assess high order loss mechanisms and potential thermal thrust components).

Of course, a validation of a full plasma jet extraction's simulation can be realised only on basis of reliable experimental measurements of relevant quantities

A proper intermediate step towards simulating the whole IEC plasma environment (with or without jet extraction) is the derivation of appropriate boundary and inflow conditions on basis of the solution of a 1D Poisson equation. However, solving the electrostatic Poisson equation needs also input parameters (e.g. particle density distributions) ideally derived from experimental measurements. This chain of dependency implies, strictly speaking, a configuration consistency between the experimental setup, the parameters put into the Poisson equation, and the simplified kinetic simulation which of course should cover the most relevant processes (e.g. ionization, charge exchange) leading to the experimental measurements. All this makes it debatable whether the presented intermediate step is a promising alternative to the full IEC jet extraction simulation.

Acknowledgements

The authors thank to ESA-ESTEC which supported this activity within the ARIADNA study 12-3201, ESA-Advanced Concepts Team.

References

[1] R. L. Hirsch. Inertial-electrostatic confinement of ionized fusion gases. Journal of Applied Physics, 38(11):4522–4534, 1967.

[2] P.T. Farnsworth. Electric discharge device for producing interactions between nuclei. US Patent 3,258,402, 1966.

[3] R.W. Bussard and N.A. Krall. Inherent characteristics of fusion power systems: Physics, engineering and economics. Journal Fusion Technology, 26:1326–1336, 1994.

[4] G.H. Miley, Y. Gu, J.M DeMora, R.A Stubbers, T.A. Hochberg, J.H. Nadler, and R.A Anderl. Discharge characteristics of the spherical inertialconfinement (iec) device. IEEE Transactions on Plasma Science, 25(4):733–739, 1997.

[5] G.H. Miley. Plasma jet source using an inertial electrostatic confinement discharge plasma, 2000.

[6] C.C. Dietrich. Improving Particle Confinement in Inertial Electrostatic Fusion for Spacecraft Power and Propulsion. PhD thesis, MIT, 2007.

[7] G.H. Miley and J. Sved. The iec star-mode fusion neutron source for naa-status and next-step designs. Journal Applied Radiation and Isotopes, 53:779–783, 2000.

[8] C. Syring and G. Herdrich. Development activities of an inertial electrostatic confinement device for space applications. 63rd IAC conference proceedings, IAC-12-C4.7-C3.5.8, 2012.

[9] G. Herdrich, U. Bauder, A. Boxberger, R.A. Gabrielli, M. Lau, D. Petkow, M. Pfeiffer, C. Syring, S. Fasoulas, Advanced plasma (propulsion) concepts at IRS, Vacuum Journal, 02/2013; 88:36-41. DOI:http://dx.doi.org/10.1016/j.vacuum.2012.02.032

[10] C. Syring, G. Herdrich, Experimental Discharge Characterization and Scaling of IEC Plasma Devices, IEPC-2013-289, 33rd International Electric Propulsion Conference, The George Washington University, Washington, D.C., USA, October 6-10, 2013.

[11] G. Herdrich, Raumfahrtrelevante Plasmen und deren anwendungsbezogene Klassifizierung, Institut für Raumfahrtsysteme, Universität Stuttgart, Mai 2012 (in German), Online Publication (OPUS): Raumfahrtrelevante Plasmen und deren anwendungsbezogene Klassifizierung, Application oriented classification of space relevant plasmas, URN: urn:nbn:de:bsz:93-opus-81408, URL: http://elib.uni-stuttgart.de/opus/volltexte/2013/8140/.

[12] T. Schönherr, F. Nees, Y. Arakawa, K. Komurasaki, and G. Herdrich, Characteristics of plasma properties in an ablative pulsed plasma thruster, Phys. Plasmas 20, 033503 (2013); http://dx.doi.org/10.1063/1.4794198 (8 pages).

[13] G. Herdrich, M. Pfeiffer, D. Petkow, C. Syring, Kinetic modelling of the jet extraction mechanism in spherical IEC devices, ARIADNA study 12-3201, ESA-ACT, final report, Oktober 2013.

[14] C. C. Dobson and I. Hrbud. Electron density and two-channel neutron emission measurements in steady-state spherical inertial-electrostatically confined plasmas, with review of the one-dimensional kinetic model. Journal of Applied Physics, 96(1):94–108, 2004.

[15] D.J. Meeker, J.T. Verdeyen, and B.E. Cherrington. Measurement of electron density in a cylindrical inertial electrostatic plasma confinement device. Journal of Applied Physics, 44:5347–5355, 1973.

[16] T.J. Dolan. Electrostatic inertial plasma confinement. Journal of Applied Physics, 43:1590–1600, 1972.

[17] T.A. Thorson. Convergence, electrostatic potential, and density measurements in a spherically convergent ion focus. Physical Plasmas, 4(1):4–15, 1997.

[18] R.M. Meyer. Inertial electrostatic confinement theoretical and experimental studies of spherical devices. PhD thesis, Faculty of nuclear engineering, University of Missouri-Columbia,USA, 2007.